RSC Advances

PAPER

View Article Online
View Journal | View Issue

Cite this: *RSC Adv.*, 2019, **9**, 41603

High residue bio-based structural–functional integration epoxy and intrinsic flame retardant mechanism study

Ji Zhou, Zhengguang Heng, Haoruo Zhang, Yang Chen, Huawei Zou* and Mei Liang

Research on structural–functional integration of polymers has become an inevitable trend and development orientation in modern materials science. An intrinsic flame-retardant epoxy with superior mechanical properties and reusability is of great application value as a composite matrix and structural material. We newly synthesized two bio-based epoxy resins, **VSE** and **VDE**, the Young's modulus of product cured by DDM (4,4-diaminodiphenyl methane) achieve 5013 MPa and 4869 MPa, respectively. The LOI values of **VSE** and **VDE** were 38.7% and 34.5% respectively and both meet UL-94 V-0 rating. High char residue at 800 °C (34.5% and 28.0%, respectively) means a superior thermal stability which conventional epoxies are unreachable. Besides, cured **VDE** have convenient processability which can be re-shape as heating up and retain complete structural performance after cooling to room temperature. Furthermore, thermogravimetric analysis coupled with infrared spectroscopy (TGA-IR) and energy dispersive X-ray spectroscopy (EDS) were used to assist scanning electron microscopy (SEM) to investigate the intrinsic flame-retardant mechanism. In this work, the effect and process of nitrogen–phosphorus synergy on flame retardant is revealed finally. These results indicate the newly prepared epoxy has excellent flame retardancy, mechanical properties and recyclability which opens new possibilities in practical applications of epoxy such as coatings, potting or composite matrix in the near future.

Received 6th October 2019
Accepted 10th December 2019

DOI: 10.1039/c9ra08098h

rsc.li/rsc-advances

1 Introduction

Due to chemical stability and processing perspectives, thermosetting resins are omnipresent in modern industrial manufacturing that requires high performing materials. In aviation and modern machinery thermosetting materials are widely employed in fiber reinforced composites which are used to manufacture structural parts due to their superior performance.[1–4] Limited by the low flame retardant, low residue and functional simplification, the conventional commercial epoxy resin diglycidyl ether of bisphenol A (DGEBA) (E51 here) will no longer adapt to the development of modern materials.[5,6] Its poor heat resistance and flammability limits its application in aerospace equipment and such harsh environments. There are two ordinary methods for improving the flame-retardant properties of materials generally, adding flame retardant into polymer matrix and introducing halogenated element into polymer molecular structure. Conventional flame retardants including ATH,[7] polychlorinated biphenyls (PCBs), polybrominated diphenyl ether (PBDEs)[8] always contain halogenated elements that are harmful to atmosphere and potentially toxic gases after burned. In 2004 and 2008, the EU had banned several types of polybrominated diphenyl ethers (PBDEs) for their latent hazards.[9–11] In a view of flame retardants addition will may lose the mechanical properties of polymers, the introduction of halogenated elements into molecular structure can avoid the decline of comprehensive performance for cured thermosetting. In this work, we used nitrogen–phosphorus synergistically to improve the flame retardancy when simultaneously raise the high temperature char residue and balanced mechanical properties. This is of great significance for the preparation of modern structural–functional integrated materials.[12]

We first prepared Schiff base bisphenol to insert nitrogen contained weak bonds into the backbone of the epoxy resin,[13] the active C=N bonds endow cured epoxy resins with a superior vapor phase flame retardancy effect, high temperature char formation and redactable ability. Due to the introduction of unsaturated bonds, the P–H bonds of 9,10-dihydro-9-oxa-10-phosphaphenanthrene-10-oxide (DOPO) can be introduced into the epoxy resin backbone by addition reaction. Recent study on phosphorus flame retardant pointed that the phosphorus-containing compounds act to stabilize the char layer during the burning process of polymers.[14] Furthermore, some studies proved that the polymer contained the imine

The State Key Lab of Polymer Materials Engineering, Polymer Research Institute of Sichuan University, Chengdu 6100652, China. E-mail: cy3262276@163.com; hwzou@163.com; Fax: +86-28-85402465; Tel: +86-28-85408288

groups CH=N brings "blowing-out" effect in burning process, while there is few works to study the synergistic effects of easy broken CH=N bonds and phosphorus-containing compounds.[15–21] In this work, we used TGA-IR and (scanning electron microscope) SEM to reveal the flame-retardant mechanism of synergy between gas and condensed phase.

Besides, the introduction of the DOPO groups supports the crosslinked network skeleton of epoxy resin, which has made two newly prepared thermoset materials undergo significant free volume changes as temperature rise. This brings excellent re-shape ability to the cured **VSE** and **VDE** which conforms to the current research direction of recyclable thermosetting resins.[22,23] In addition, vanillin, an important raw material in this synthesis process, is a compound derived from lignin which is the second most abundant natural organic material and which conforms to the development trend of green chemistry. For **VSE**, the Schiff base endow it with good corrosion inhibition and passivation performance for steel, copper and aluminum. These superior flame retardant, high char residue properties, convenient processability and high mechanical modulus promotes **VSE** and **VDE** to have great application prospects in the field of fireproof adhesives, flame-retardant potting and modern structural polymer material.[24,25] Simultaneously, the use of vanillin as a bio-based building-block for polymer chemistry and the recycling characteristics of cured **VSE** and **VDE** endow this work with great significance to design future green thermosetting resins.[26–28]

As following works, the intermediates of **VSE** is synthesized from vanillin and *p*-hydroxybenzaldehyde, and the intermediates of **VDP** was added DOPO to obtain phosphorus-containing difunctional diphenols. The bisphenol intermediate is then reacted with an excess of epichlorohydrin with phase transfer catalyst to obtain corresponding epoxy resins.[29] Molecular structure was characterized by (Fourier-transform infrared spectroscopy) FTIR, (nuclear magnetic resonance) ^{1}H-NMR, and mass spectrometry (ESI-MS). DDM was used as curing agent to prepared cured solid samples, the curing behavior were investigated by differential scanning calorimetry (DSC). The thermal stability of cured **VSE** and **VDE** was characterized by thermogravimetric analysis (TGA). Flame retardancy and flame retarding mechanism of the epoxy resins were investigated by vertical burning and limit oxygen index test and TG-FTIR. The surface morphology and elemental composition of char layer were analyzed by scanning electron microscope coupled energy dispersive X-ray spectroscopy (SEM-EDS).[30] Besides, the molecular dynamics (MD) models were employed to describe the microstructure of cured resins for re-shape ability.

2 Experimental

2.1 General

Absolute ethanol and benzyltrimethylammonium chloride (TMBAC) were provided by Chengdu Chron Chemicals Co., Ltd China. Vanillin, *p*-aminophenol, epichlorohydrin (ECH) obtained from Aladdin-reagent Co., China. 4,4-diaminodiphenylmethane (DDM) was provided by Guangdong Wengjiang Chemicals Co., China. 9,10-Dihydro-9-oxa-10-phosphaphenanthrene 10 – oxide (DOPO) was provided by Shanghai Meryer Co., LTD., China. DGEBA (ECH = 0.51) was provided by Nantong Xingchen Synthetic material Co., LTD., China. All reagents were not specially purified.

The ^{1}H NMR spectra were recorded on Bruker AV II (Switzerland) at 600 MHz with TMS as an internal standard and DMSO-d_6 as solvent. FTIR and TGA-FTIR were measured with NICOLET 570 and Nicolet iS50 (NICOLET, America). Liquid chromatography-mass spectrometry (LC-MS) were recorded on Finnegan TSQ Quantum Ultra (Thermo Fisher Scientific, America). Epoxy value were measured with hydrochloric acid–acetone titration method, hydrochloric acid and acetone were mixed in a volume ratio of 1 : 40, then used 0.1 mol L^{-1} sodium hydroxide solution for blank test and the control test titration. Approximately 5 mg pre-curing mixture for DSC measurements, which were on a NETZSCH 204-F1 (NETASCH, Germany) at 2.5, 5, 7.5, 10 K for curing process kinetics. Cured samples with dimension of 800 × 100 × 4 mm were used for the three-point bending test at 2 mm min^{-1} and a span of 64 mm (Instron 5567) according to GB/T 2570-1995. The cured product decomposition temperature and residue were investigated by a TG290-F1 (NETZSCH, Germany) under a nitrogen atmosphere, which were heated from 40 to 800 °C. The Izod impact test was performed with a 1 J pendulum and the sample dimension of 800 × 100 × 4 mm by XJU-55 (Chengde Jinjian Instrument Company, China) according to GB/T 1843-2008. The dynamic mechanical analysis (DMA) samples with dimensions of 60 × 10 × 4 mm were mounted on a three-point bending device with a span of 20 mm, the frequency was set as 1.0 Hz to test glass transition temperature (T_g) (TA Instrument, America). Limit oxygen index test (LOI) were performed on NF-3 oxygen index instrument (Nanjing Jiangning Analysis Instrument Company, China) with sample dimensions of 80 × 10 × 4 mm according to ISO 4589-2. UL-94 vertical burning tests were tested on a vertical burning tester with sample dimensions of 80 × 10 × 3 mm. Then taking char layers after LOI test for morphology analysis, observed the front and backside of frontmost char layer and adjacent surface of front residue by scanning electron microscopy JSM-7500F (JEOL, Japan). Then selected the scanning surface for energy dispersive X-ray spectroscopy (EDS) (Oxford Instrument, Britain). The reshaping spline is poured in a PTFE mold, and the cured samples size are 12 × 180 × 2 mm.

2.2 Synthesis of 4-hydroxy-*N*-(4-hydroxy-3-methoxybenzylidene)aniline (Vscb)[31]

Vscb was synthesized *via* condensation reaction with vanillin and *p*-aminophenol, accompanied by side reaction of water. Dissolve vanillin (0.1 mol) and *p*-aminophenol (0.09 mol) in 150 ml ethanol, respectively. Pouring the *p*-aminophenol solution into a three-necked flask with a magnetic stirrer and a reflux condenser and slowly drop the vanillin solution into vessel. The reaction was carried out at 90 °C for 3 hours. Rotary distillation to concentrated reaction mixture and recrystallization under 10 °C for more than 6 hours and filtered to give a yellow solid. Washing with deionized water and recrystallization in dilute ethanol (ethanol : water = 1 : 1) overnight.

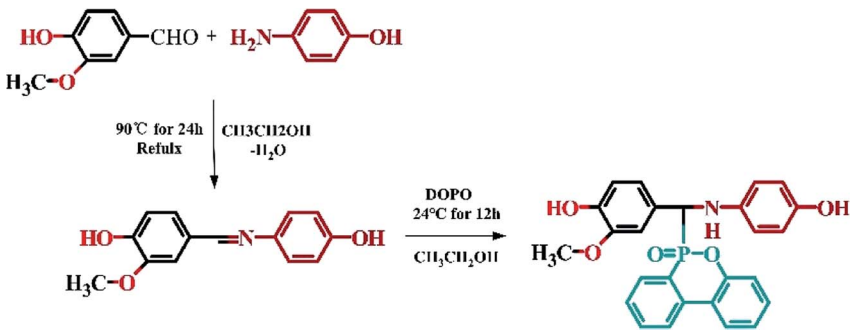

Scheme 1 The synthesis of **Vscb** and **VDP**.

Yellow crystal was collected by filtration and dried at 80 °C in a vacuum oven overnight. Product weighed 21.52 g, yield is about 92%. The procedure of synthesis for vanillin Schiff base intermediate was shown in Scheme 1.

FTIR (KBr): ν^{Methoxy}(Ar–O) = 1283 cm^{-1}, $\nu_{(C=N)}$ = 1622 cm^{-1}, $\nu_{(O-H)}$ = 3301 cm^{-1}.

^{1}H NMR (600 MHz, DMSO-d$_6$, ppm): δ 9.64 (s, 1H), 9.41 (s, 1H), 8.43 (s, 1H), 7.48 (d, J = 1.8 Hz, 1H), 7.27 (dd, J = 8.1, 1.8 Hz, 1H), 7.15–7.09 (m, 2H), 6.87 (d, J = 8.1 Hz, 1H), 6.80–6.74 (m, 2H), 3.84 (s, 3H).

2.3 Synthesis of 9-[(3-ethyl-4-hydroxyphenyl)[(4-hydroxyphenyl)amino]methyl]-8-oxa-9λ^5-phosphatricyclo[8.4.0.0^{2,7}]tetradeca-1(14),2(7),3,5,10,12-hexaen-9-one (VDP)[29]

VDP was produced by the addition reaction of DOPO and **Vscb**. Weighed **Vscb** (0.075 mol) and dissolved in 100 ml ethanol, then poured into a round-bottomed flask with a magnetic stirrer. DOPO (0.075 mol) was ground into fine powder and added to the reaction vessel while reacting at room temperature for 24 h. After the reaction was over, the mixture was poured into deionized water and stirred for 2 h. Ageing the mixture and filtration, 21.35 g light yellow solid was collected and dried at 90 °C for 6 hours in a vacuum oven, the yield rate is about 90%. The procedure of synthesis for **VDP** intermediate was shown in Scheme 1.

FTIR (KBr): ν(P–O) = 950 cm^{-1}, ν(P=O) = 1276 cm^{-1}, ν(Ar–N) = 1224 cm^{-1}, ν(N–H) = 3314 cm^{-1}.

1H NMR (600 MHz, DMSO-d$_6$,ppm): δ 8.86 (s, 1H), 8.22–8.13 (m, 2H), 7.80–7.66 (m, 2H), 7.50–7.40 (m, 2H), 7.31 (qd, J = 7.6, 1.3 Hz, 1H), 7.18 (dd, J = 8.1, 1.3 Hz, 1H), 6.90 (dt, J = 4.1, 1.8 Hz, 1H), 6.76–6.68 (m, 1H), 6.62–6.50 (m, 2H), 6.52–6.45 (m, 1H), 6.44–6.34 (m, 2H), 5.12 (dd, J = 17.6, 10.1 Hz, 1H), 3.67 (s, 1H), 3.62 (s, 2H).

2.4 Synthesis of Schiff base epoxy resin (VSE) and DOPO addition Schiff base epoxy resin (VDE)[31]

The optimum reaction conditions were as follows: the molar ratio of bisphenol (**Vscb** Or **VDP**), epichlorohydrin to TMBAC was 10 : 400 : 0.5, the reaction time is 24 h, the reaction temperature is 90 °C. Extracting the catalyst with using deionized water for three times. Retain epoxy resin and epichlorohydrin mixture, removal excess epichlorohydrin by rotary evaporation. The product was dried in a vacuum oven for 12 hours to remove residual epichlorohydrin. The procedure of synthesis for **VSE** and **VDE** was shown in Scheme 2.

FTIR (**VSE**): ν(C=N) = 1622 cm^{-1}, ν(O–H) = 3439 cm^{-1}, ν^{epoxy}(C–O–C) = 914 cm^{-1}.

FTIR (**VDE**): ν^{epoxy}(C–O–C) = 908 cm^{-1}, ν(O–H) = 3429 cm^{-1}.

2.5 Preparation of the cured epoxy resins

Both epoxy resins used DDM as a curing agent, and mixed with epoxy resin in a 1 : 1 ratio. (Epoxy value determination using hydrochloric acid–acetone method. Configured 80 ml hydrochloric acid–acetone in a volume ration 1 : 40. Divided into four

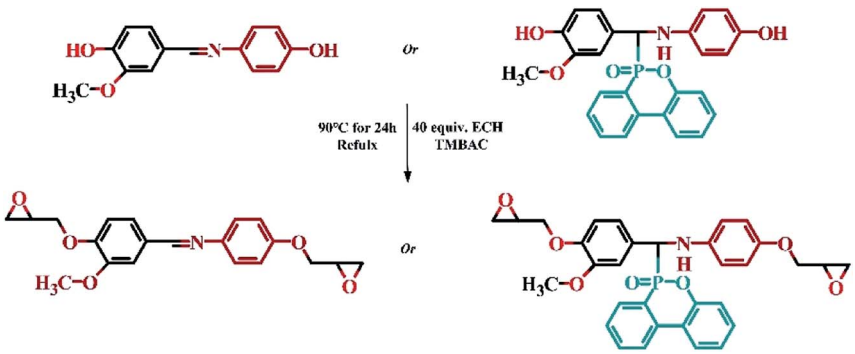

Scheme 2 The synthesis of **VSE** and **VDE**.

parts, separately added two epoxy resins and diglycidyl ether of bisphenol A (DGEBA) with 0.3–0.6 g, and set a blank titration. Added methyl red indicator and titration with 0.1 mol L^{-1} sodium hydroxide standard solution.) The liquid mixture was stirred at 90 °C and poured into a PTFE mold. And staged curing at 100 °C for 1 hour, at 135 °C for 3 hours and 180 °C for 2 hours. Obtained rectangular samples with dimensions of 80 mm × 100 mm × 4 mm. Then placed the samples in oven natural cooling for annealed. Cured DGEBA sample used the same curing conditions as a comparison.

3 Result and discussion

3.1 Synthesis and characterization of Vscb, VDP, VSE and VDE

VSE and **VDE** used the same prepared method and the polymerization degree was about 1–2 which were calculated from the epoxy value obtained by titration. Since the synthesis of **Vscb** is a Schiff base condensation reaction using a slight excess of vanillin with an aromatic amine, two recrystallization purifications are required after the reaction. The synthesis of product obtained by addition reaction between **Vscb** and DOPO meet the requirements for direct further reaction so that it can be directly used for the preparation of epoxy resin.

The chemical structure of all the product obtained in this work were characterized by ^{1}H NMR, FT-IR and MS. In Fig. 1 of FTIR spectra, the peaks at 3301 cm^{-1}, 3439 cm^{-1}, 3424 cm^{-1}, 3429 cm^{-1} belong to O–H of **Vscb**, **VSE**, **VDP** and **VDE**. The peak at 1622 cm^{-1} belong to C=N of Schiff base with **Vscb** and **VSE**. Peaks at 1276 cm^{-1} ascribed to P=O and 950 cm^{-1} ascribed to P–O of DOPO group. In this FTIR spectra, the O–H were assigned to epoxy resin backbones, and the peaks of epoxy groups for C–O–C in **VSE** and **VDE** were showed at 914 cm^{-1} and 908 cm^{-1}, respectively. The appearance of the epoxy group peaks in FTIR spectra means that the two compounds are successfully etherified. In Fig. 2 of ^{1}H NMR of **Vscb** and **VDP**, the chemical shift and the integral area are well matched to the structure of the two compounds.

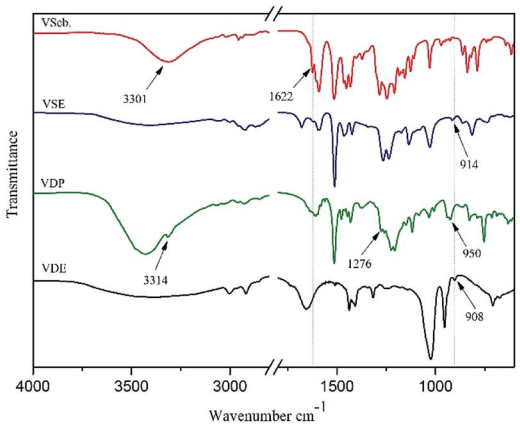

Fig. 1 FTIR spectra of **Vscb**, **VSE**, **VDP** and **VDE** scanned from 500–4000 cm^{-1}.

The MS spectrum of intermediate is derived from TIC and the relative time is at which the peak appeared. Fig. 3 shows the ESI-MS spectrum of **Vscb** and **VDP**. From the primary fragmentation peak, it can be seen that the molecular structure of the synthesized product is as expected. The mass spectrometry demonstrates the successful synthesis of **Vscb** and **VDP**.

3.2 Curing kinetics

The curing process of **VSE** and **VDE** with DDM is investigated by non-isothermal DSC test. And the obtained data is calculated according to the Kissinger method (eqn (1)) to calculate the pre-exponential factor and apparent activation energy.[32] The study of curing kinetics is used to describe the difficulty of the epoxy resin in the curing process, which reflects the impact of the main chain structure of epoxies to some extent in the curing process.

$$\ln\left(\frac{\beta_i}{T_{pi}^2}\right) = \ln\frac{A_k R}{E_k} - \frac{E_k}{R}\frac{1}{T_{pi}} \quad (i = 1, 2, 3, 4) \tag{1}$$

where β_i is heating rate, T_{pi} is the exothermic peak temperature, E_k is Kissinger's activation energy, R is gas constant, A_k is the pre-exponential factor. Plotted by $\ln\left(\frac{\beta_i}{T_{pi}^2}\right)$ to $\frac{1}{T_{pi}}$ and linearly fit. E_k can be calculated by the slope and A_k can be calculated by the line intercept. The concluded E_k, A_k and the raw data are listed in Table 1.

Both data meet Pearson's r well. In the obtained results of reaction activation energy, the E_k value of **VSE** is much higher than **VDE**. Which reflects that **VSE** requires higher energy during the curing process, extra energy is likely to be used to overcome the forces between the **VSE** molecular chains which may from hydrogen bonds formed by intermolecular interactions. This shows that the regular **VSE** molecular chain has strong polarity, the curing reaction can proceed only after obtaining higher energy. The introduction of DOPO groups breaks the regularity of the **VDE** molecular structure that makes **VDE** can be cured more easily.

3.3 Thermal stability and decomposition mechanism analysis

The char residue ratio and decomposition temperature to 800 °C are used to describe the high temperature thermal stability of cured **VSE** and **VDE**. Fig. 4 shows the TGA and DTG curves of cured **VSE** and **VDE** with DDM under N_2. The data is summarized in Table 2. Existing research proved that the thermal decomposition course of conventional epoxy resin DGEBA can be classified as breakage of weak bonds, formation of phenol, decomposition of benzene rings.[33] Cured **VSE** and its derivative resins **VDE** have approximative decomposition peaks at about 265 °C and 325 °C which corresponds to the break of the Ar–C–N and the CH_3–O–Ar, respectively. This result was inferred by comparing to the thermal decomposition test of the epoxy resin extra prepared in previous work (the same series of epoxy resins prepared by *p*-hydroxybenzaldehyde replaced vanillin). The decomposition peaks at 279 °C for **VSE**

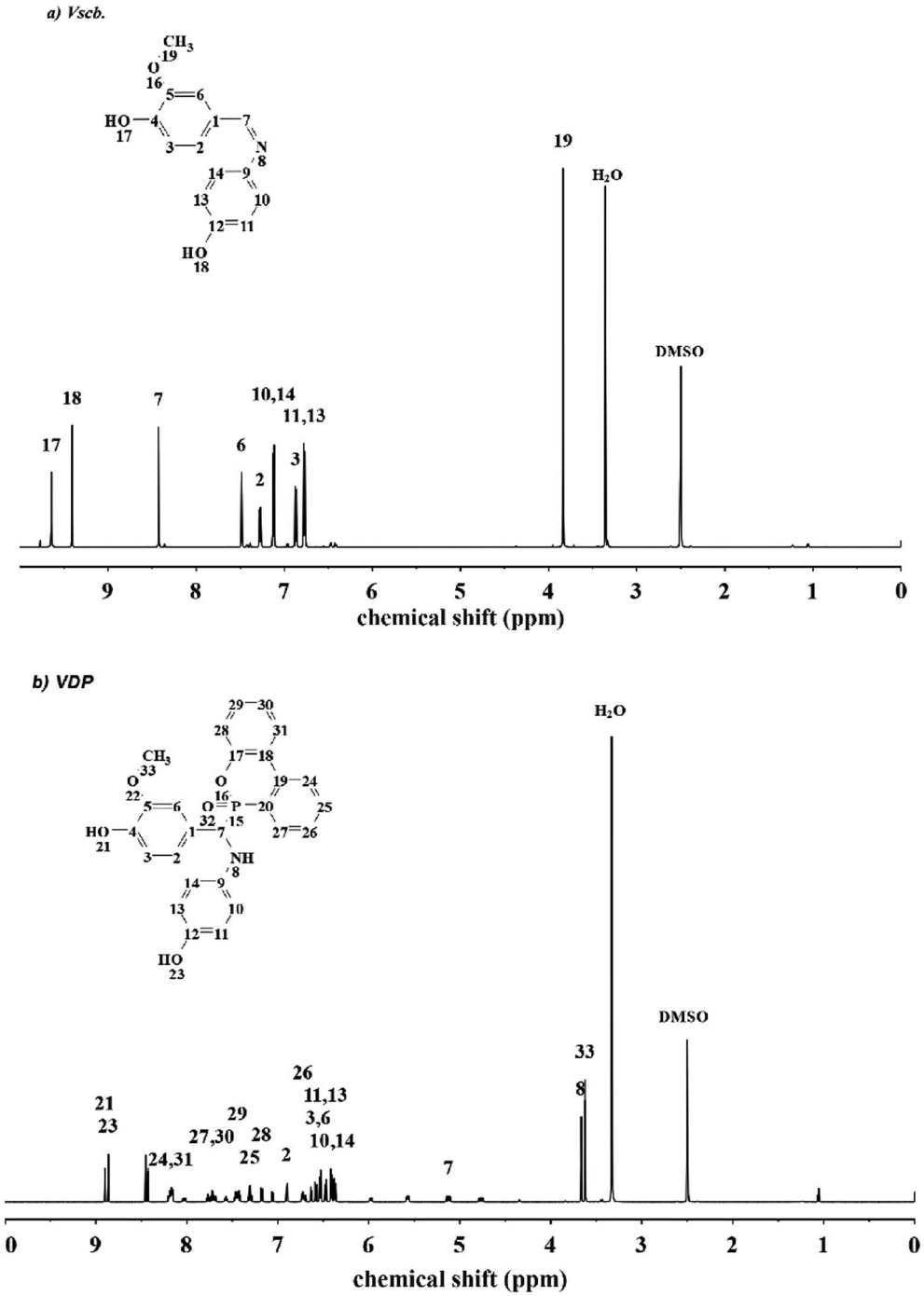

Fig. 2 ^{1}H NMR spectra of (a)**Vscb** (b)**VDP** after purification, DMSO-d_6 as solvent.

corresponds to the break of Ar–N. The lower $T_{d4\%}$ in the DTG curve for **VDE** was ascribed to the fact that the O=P–O bonds in epoxy resin was more apt to degrade than C–C bond. On the other hand, the peaks after 325 °C belonging to **VDE** is due to the self-degradation of the DOPO groups. This results confirms that the epoxy resin with nitrogen in the main chain will undergo chain decomposition at a lower temperature more easily, and this is one of the reasons for the nitrogen-containing epoxy resin has a vapor phase flame retardant mechanism.[33] The gas product in the decomposition process of cured epoxies will be corroborated by TGA-IR as following.

The residue of **VSE** and **VDE** achieved 34.5% and 28.0% at 800 °C, which of cured DGEBA is only 11.8%. Both newly prepared nitrogen-containing and phosphorus-containing epoxy resins have higher residue than DGEBA. The introduction of these readily cleavable chemical bonds in **VSE** and **VDE** molecular structure containing nitrogen and phosphorus allows them to break concentratedly at high temperatures and

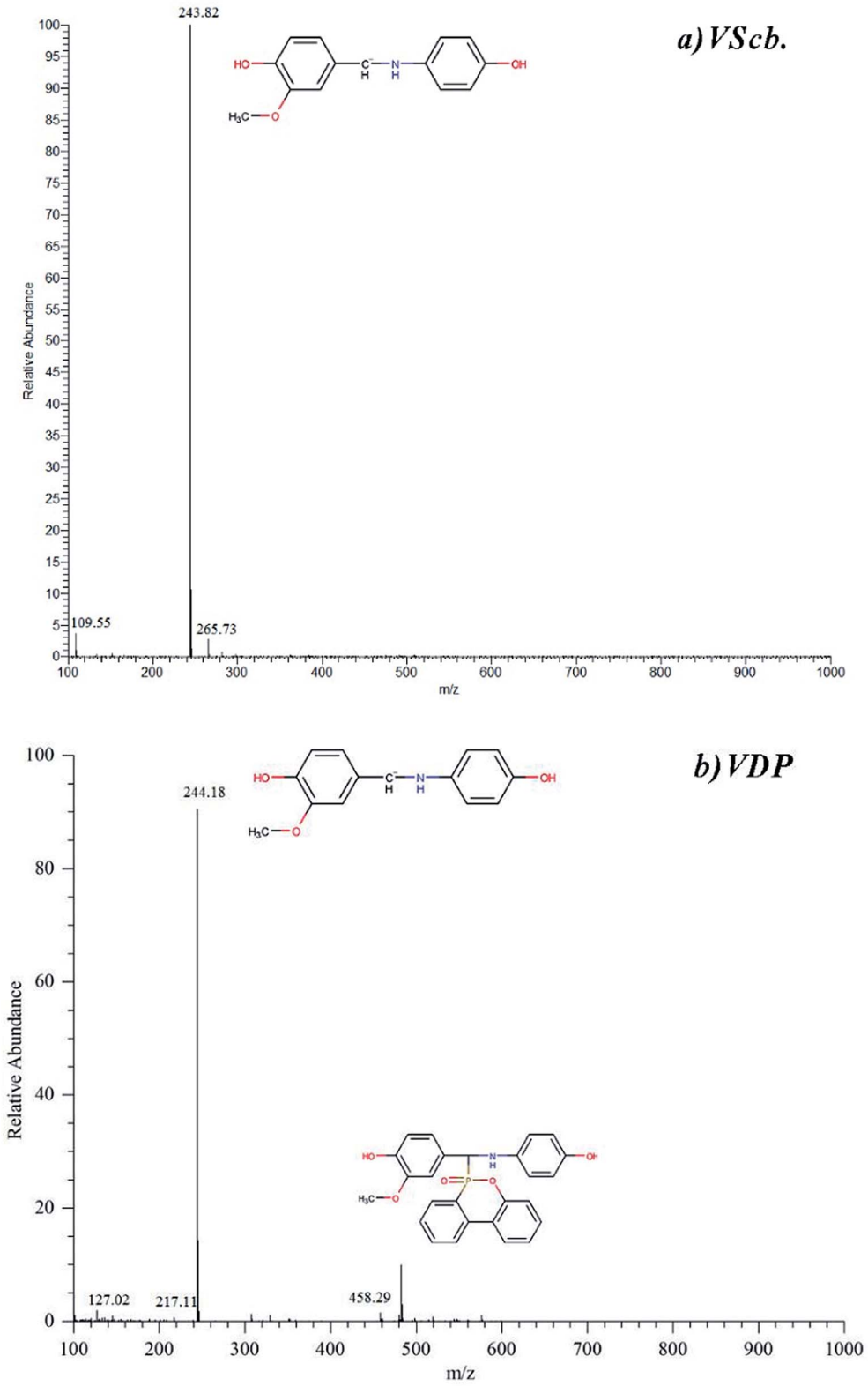

Fig. 3 ESI-MS spectra of (a) **Vscb** (b) **VDP**, data from LC-MS, the separating resolution for chromatographic peak is good.

leaving more aromatic ring structures which are more easily to form stable carbon residues. Therefore, cured **VSE** and **VDE** have lower decomposition temperatures than that of DGEBA while saving more char residue. It can be seen from Fig. 5(a) that there are more volatile organic compounds (VOCs) that escape from cured E51 during decomposition, the compounds

Table 1 The pre-exponential factor & activation energy of VSE and VDE during curing process

Sample	Slope	Intercept	A_k/s^{-1}	E_k/J mol^{-1}	Pearson's r
VSE-DDM	−1384.64	−0.66	716.91	11 511.87	0.9977
VDE-DDM	−336.39	−5.68	1.14	2796.78	−0.9527

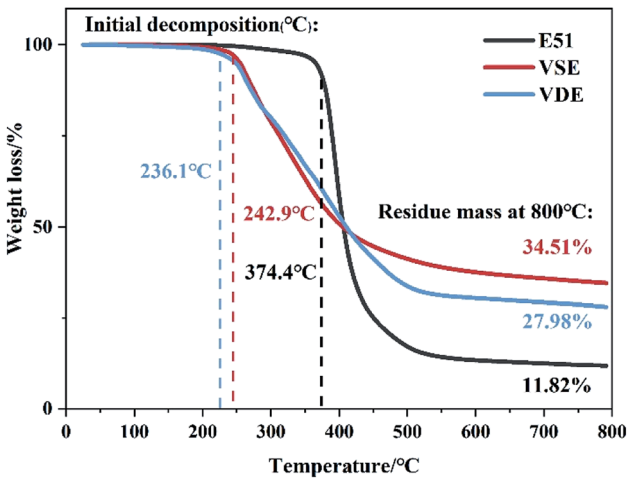

Fig. 4 TG and DTG curves for cured DGEBA, VSE and VDE from 40 °C to 200 °C under N_2, purge gas velocity is 100 ml min^{-1}.

escaped after 48 min at 2900 cm^{-1} is mainly assigned to various kinds of saturated alkanes, the compounds over 3000 cm^{-1} is mainly assigned to aromatic compounds. The peaks at about 2250 cm^{-1} were can be observed from Fig. 5(a), (b) and (c) and they are assigned to nitrogen-containing compounds escaped. There is no significant signal peak at about 270 °C since escaped N_2 which cannot be measured by IR. It can also be observed from Fig. 5(c) at about 1250 cm^{-1} that there are phosphorus-containing compounds in escaped gas from 31–60 min. Fig. 5 is an important proof for that the cured **VSE** and **VDE** has superior ability to reduce the production of VOCs during decomposition.

The isopropyl groups in the middle of the benzene ring of DGEBA has a higher molecular mass than C=N groups, and it is not only impossible to concentrate the energy in crosslinked network decomposed process, but also take off more residual mass in the form of VOCs when decomposition occurred. A lower char residue for **VDE** than **VSE** is mainly due to the mass loss caused by sublimation of phosphorus compounds at high temperatures.[34,35]

3.4 Mechanical properties

The results of three-points bending test, T_g and impact strength are presented in Table 3. It can be seen from Fig. 6(b) that the modulus of cured **VSE** and **VDE** has been greatly improved compared to cured DGEBA. The bending strength of cured **VSE** achieve 154 MPa which ascribed the better configuration of the **VSE** molecular chain and the more polar C=N bonds. This causes cured **VSE** to form more amounts of hydrogen bonds during the cross-linking process, resulting in a denser cross-linked network and this is also an important reason for the cured **VSE** to obtain a higher modulus. For cured **VDE**, in addition to having more polar chemical bonds, the side chains structure with high rigidity is one of important reasons for the higher modulus of cured **VDE**.[16,36] The microstructure changes in the crosslinked network have greatly improved the modulus of the two epoxy resin cured products, while the high rigidity has caused the fracture toughness to decrease.

The T_g of cured DGEBA, **VSE** and **VDE** are 173.9, 176.1 and 129.6 °C, respectively. A more regular structure and more polar chemical bonds additionally endow cured **VSE** with a higher T_g. These crystal-forming epoxy resin molecules are rearranged during curing and cause the cured **VSE** to have a higher cross-linked density. Different from **VSE**, the regularity of **VDE**'s crosslinked network was broken after the DOPO groups were introduced into the skeleton and the larger steric hindrance also limits the curing behavior of **VDE**.

3.5 Flame retardant results and char layer morphology analysis

The flame retardancy was investigated by vertical burning test and limit oxygen index (LOI). LOI value and UL94 rating as the standard to evaluate the flame-retardant performance for E51, **VSE** and **VDE** under the same curing conditions. In can be observed from the vertical burning test that there is not fused drop generated when cured epoxy were burning. The flame retardancy of both newly prepared cured epoxy reached UL94 V-0 level, this proves that these two cured epoxy resins have excellent intrinsic flame retardancy. The LOI values of cured **VSE** and **VDE** reached 34.5% and 38.7%, respectively. Benefit from excellent char layer formation ability, **VSE** and **VDE** can prevent the formation of droplets during combustion process. Conventional epoxy resin DGEBA cured sample cannot meet the requirements of flame-retardant standards while the limiting oxygen index value was only 24.3%. These evidences prove that two newly prepared epoxy resins **VSE** and **VDE** cured samples have excellent flame retardancy. Fig. 6(a) presents the difference in LOI values for the three epoxy resins, it can be seen that the

Table 2 TGA and DTG data of the cured VSE and VDE

	T_{1st} (°C)	T_{2nd} (°C)	T_{3rd} (°C)	$T_{d5\%}$ (°C)	$T_{d30\%}$ (°C)	Residue$_{800}$ (%)
E51-DDM	385.5	—	—	369.9	386.7	11.8
VSE-DDM	265.8	279.1	324.2	254.9	328.5	34.5
VDE-DDM	261.8	275.65	326.8	248.8	339.2	28.0

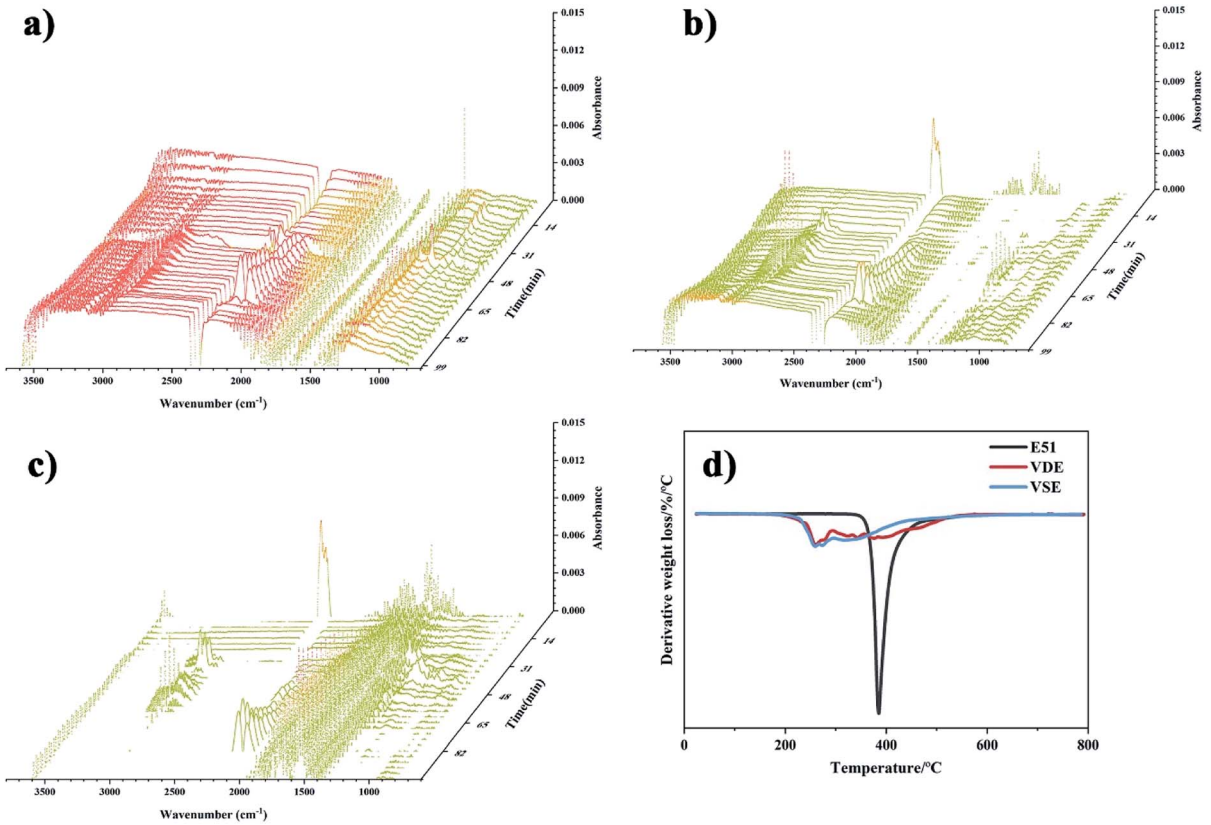

Fig. 5 Time dependent FTIR waterfall curves of cured (a) E51, (b) **VSE** and (c) **VDE** combined with (d) TGA curves. The sampling interval is 40.84 s, the IR scanning range is from 400 to 4000 cm^{-1} and the temperature range for TGA is from 40 to 800 °C.

flame retardancy of **VSE** and **VDE** has been greatly improved by molecular structure design.

There are two main reasons for the promotion of flame retardancy for cured **VSE** and **VDE**. The first is the vapor phase flame retardant mechanism which was caused by the introduction of nitrogen contained weak bonds into the main chain. The second is the condensed phase flame-retardant mechanism which was caused by the introduction of phosphorus compounds. Nitrogen will escape from crosslinked network as N_2 or NH_3 when the cured resin is decomposing, these escaped gasses take away the heat generated and have an effect on cooling burning part of resins. Besides, the flame during combustion may be blown out by the gas emitted. Therefore, this phenomenon occurring in the combustion process was named as the "blowing out" according to the study on gas generated mechanism of polymers during combustion.[23] The introduction of phosphorus enhances the ability to stabilize the char layer which can be proved by the result of time dependence FTIR spectrum obtained from TGA-FTIR, the VOCs few escaped from decomposition of cured epoxies so that it presents a lower absorbance in Fig. 5(c). The thermal insulation barrier generated by a polymeric layer of charred phosphoric acid will stop spreading of the flame. Fig. 7 shows SEM photographs of the frontmost char layer of residue after LOI test. It can be observed form SEM photos that the vapor phase and the condensed phase were synergy in combustion process of cured **VDE**.

Fig. 7 present the morphology of the frontmost char layer of cured E51, **VSE** and **VDE** after combustion. It can be determined that the introduction of DOPO as side chains has a huge visible effect on stabilizing char layer. For that of cured **VSE**, the morphology of char layer is rougher, larger pores are collected on the surface of front char layer, these micropores play an important role for rapidly escaped gas. The introduction of phosphorus-containing compounds results a denser char layer

Table 3 Mechanical properties and T_g of cured E51, **VSE** and **VDE**

Name	Bending stress (MPa)	Bending modulus (MPa)	Impact strength (kJ m^{-2})	T_g (°C)
E51-DDM	105.9 ± 2.2	2554 ± 98	22.7 ± 0.4	173.9
VSE-DDM	154.0 ± 3.5	5013 ± 154	8.2 ± 0.6	176.1
VDE-DDM	54.9 ± 4.1	4869 ± 105	1.9 ± 0.3	129.6

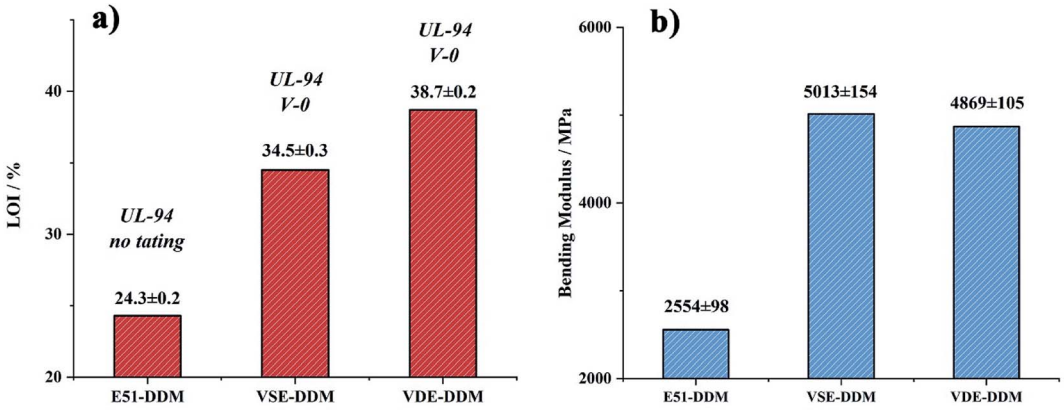

Fig. 6 Column chart of (a) LOI values and UL94 rating (b) Young's modulus for cured E51, VSE and VDE.

for **VDE**, the smaller micropores and reduced roughness make the char layer more stable and it would not be easily blown off by the airflow. To verify if phosphorus is really effective in stabilizing the char layer, the reverse side of the residual char layer was also observed as following.

It can be seen from Fig. 8 that the backside char layer from **VDE** after combustion has a high degree of pore connection and lower hole depth compared to that of **VSE**. Fig. 9 show the morphology of adjacent surface below the frontmost layer for **VSE** and **VDE** which were collected after LOI test. The above phenomenon proved that some compounds produced by the introduction of DOPO accelerated the crosslinked of epoxy degradation products to form more stable and compact char residues rich in organophosphorus compounds. The gas usually escapes in the form of NH_3 and N_2 and take away a lot of heat which has been confirmed in the above.[37] Under the effect of phosphorus, the adjacent surface below the frontmost layer in Fig. 9 exhibits mores stability which is essential to prevent more VOCs from being produced.

In order to investigate the composition of the frontmost char layer and the adjacent surface below the frontmost layer, EDS analysis was performed on the SEM scanning surface. Fig. 10 shows the EDS spectrum to characterize the element distribution. Table 4 conclude the elemental content data from the EDS spectrum of **VSE** and **VDE**. By analyzing the data in Table 4 reveals that the char layer element composition of the cured E51

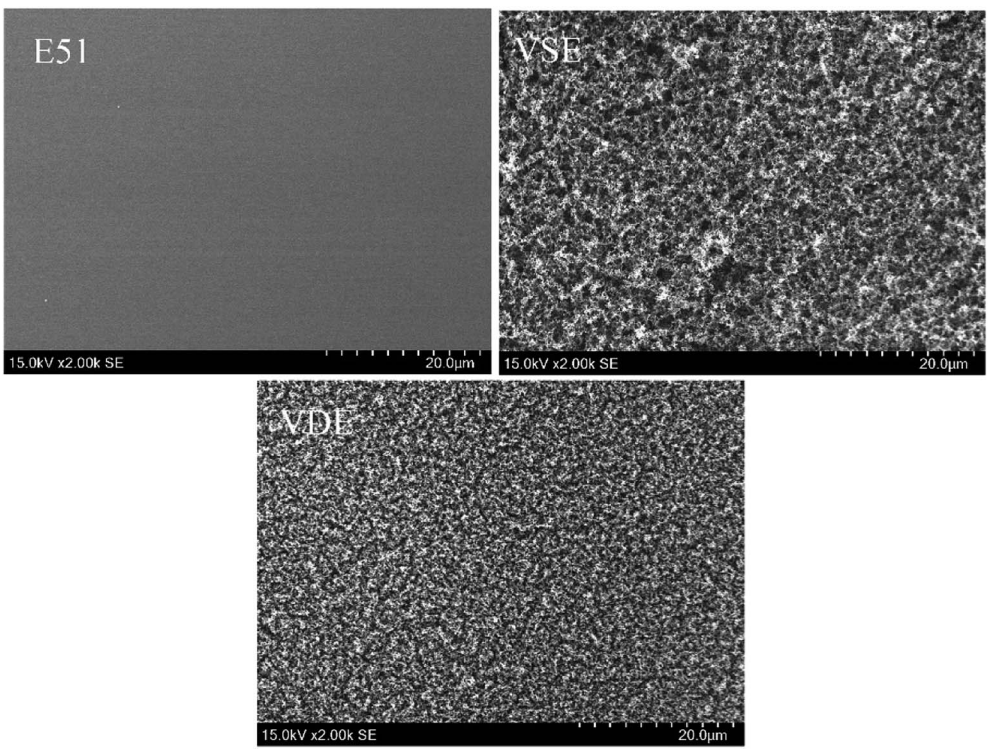

Fig. 7 SEM photographs of the frontmost char layer.

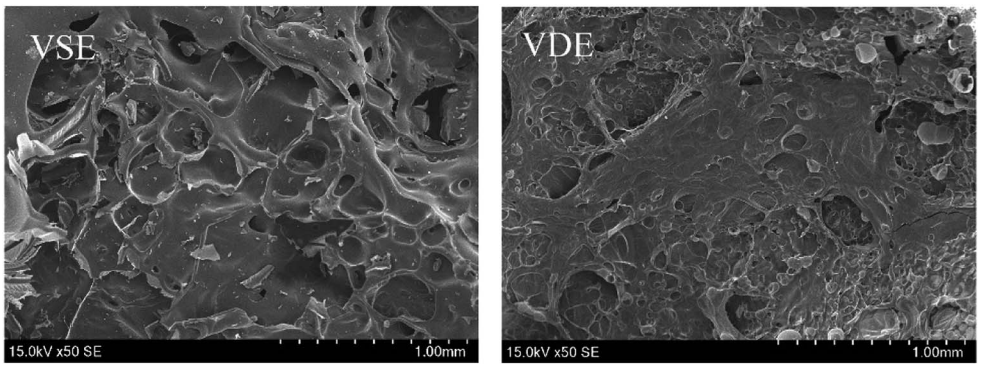

Fig. 8 SEM photographs of the backside of frontmost char layer.

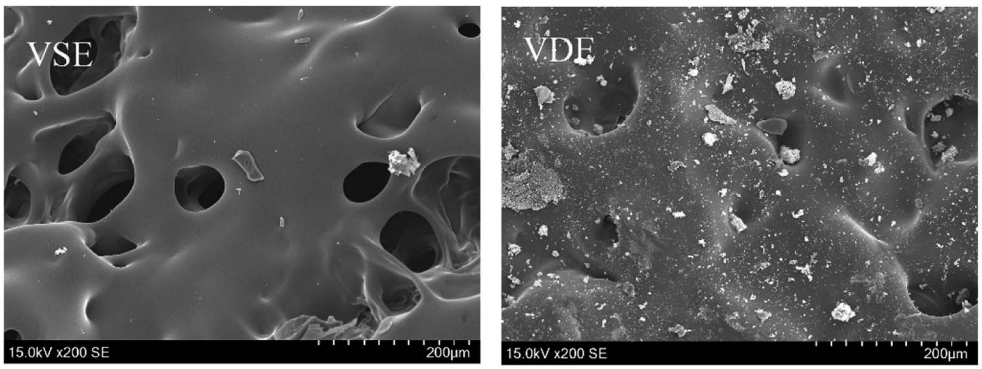

Fig. 9 SEM photographs of adjacent surface below the frontmost layer.

from the residue after combustion is approximative to the surface below the char layer in addition to the presence of phosphorus. The carbon content of the **VSE** residue char layer is significantly higher than that of the surface below the frontmost layer, which shows that the char formation ability of decomposition products was improved after nitrogen escaped. In the EDS spectrum after **VDE** combustion, it was found that the content of phosphorus on the char layer from the residue was

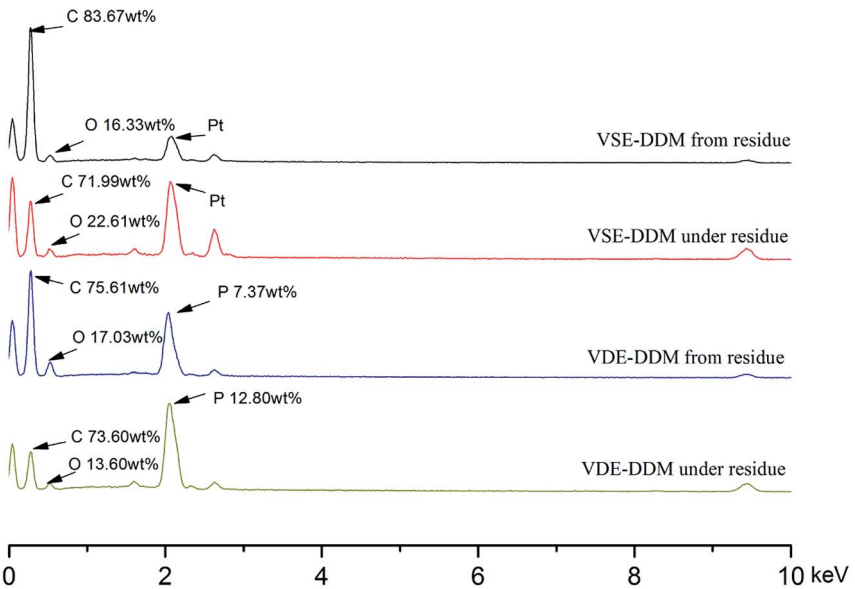

Fig. 10 EDS spectrum of char layer from the residue and the adjacent surface below the frontmost char layer.

Table 4 The elements composition of char layer from residue and the adjacent surface below the frontmost char layer

	Char layer from residue			Char layer under residue		
Sample (wt%)	Carbon content	Oxygen content	Phosphorus content	Carbon content	Oxygen content	Phosphorus content
E51-DDM	76.17	23.83	—	73.35	26.65	—
VSE-DDM	83.67	16.33	—	71.99	28.01	—
VDE-DDM	75.61	17.03	7.37	73.60	13.60	12.80

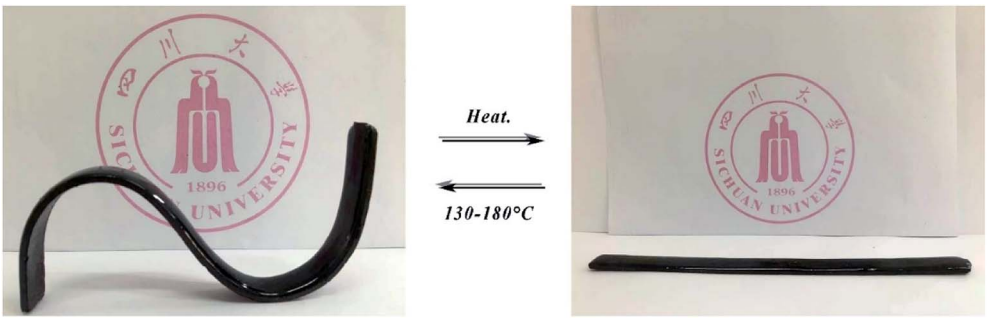

Fig. 11 A photo of the epoxy resin cured spline reshaped after heating.

lower than that of the char layer under the residue. This demonstrated that some organophosphorus compounds exited in the surface below frontmost char layer after burning while the frontmost layer was accompanied by the process of phosphorus sublimation.

3.6 Re-shape ability for cured VDE

Fig. 11 showed a photograph of the **VDE**-DDM cured spline reshaping and restoring shape after heating up. In general, epoxy resin cured sample with high modulus are difficult to reshape after heating. Cured **VDE** spline can be repeatedly reshaping multiple times after heating up, and maintains stiffness and shape when it returns to room temperature. This allows **VDE** to have shape retention characteristics that cured E51 and **VSE** does not own. There are several reasons for analyzing the molecular structure and epoxy resin cured crosslinking network. Firstly, the reason for **VSE** does not have reshape ability is that the C=N bonds limits the rotational motion of the Ar–O in the epoxy segment. Secondly, the binding of hydrogen bonds makes the cured **VSE** crosslinked network denser and has higher cross-linking degree. Finally, the introduction of dangling chains extends the crosslinked network of **VDE**-DDM, so that the crosslinked network of cured **VDE** received "dilution". The shape memory effect of **VDE** allows it to be shaped without heating into viscous-flow state like thermoplastic under high temperature which endows it great application prospects in deformable flame-retardant polymer materials.

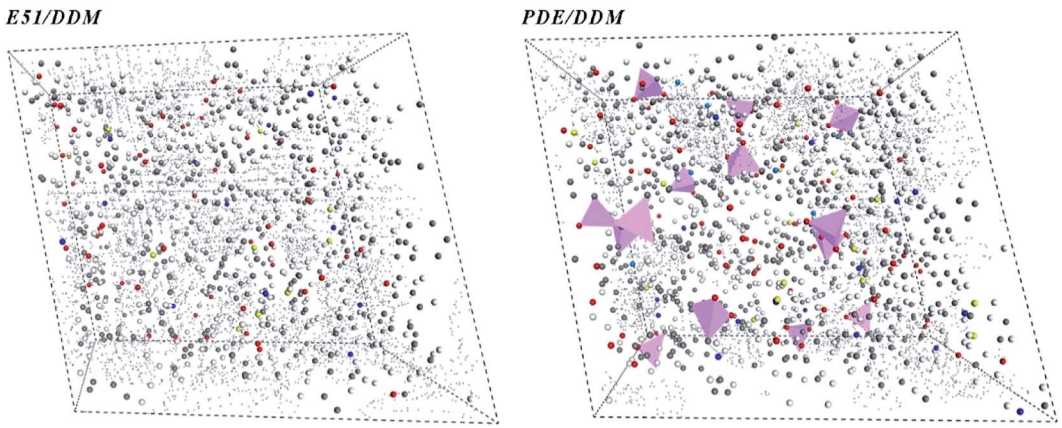

Fig. 12 DGEBA/DDM and **VDE**/DDM amorphous cell model by molecular dynamics (MD) simulation.

According to the MD simulation, we used Monte-Carlo method to mix **VDE** molecules and DDM molecules in a molar ratio of 1 : 1, and established a solidified **VDE** model by an automatic cross-linking procedure. After performing Connolly surface statistics, we obtained free volume distribution maps of DGEBA/DDM and **VDE**/DDM cells under periodic conditions. Black dots scattered in Fig. 12 represent the free volume voids of the cured epoxies, pink triangular pyramids represent occupied side chains of DOPO. Black spots are denser in the DGEBA/DDM cured cells center as long as there are no bulky side groups occupying the volume. It can be inferred that the **VDE**/DDM has a smaller free volume cavity due to the occupation of the bulky side chains. This brings a higher modulus to the **VDE**/DDM system and reducing the crosslinked density for **VDE**/DDM cured system. Therefore, as the temperature increases, the **VDE**/DDM system has more convenient processability compared to cured DGEBA. Besides, cured **VDE** would still maintain excellent mechanical properties after multiple times reshaping.

4 Conclusions

These two newly prepared epoxy resin **VSE** and **VDE** were synthesized by etherification of epichlorohydrin and their cured products possess superior structural–functional integrated characteristic. Both cured samples achieved UL94 V-0 ratio, the LOI values of **VSE** and **VDE** achieve 34.5% and 38.7%, respectively. For **VSE**, the introduction of C=N bonds endow it with excellent flame retardancy which is caused by a vapor phase mechanism. For **VDE**, the introduction of DOPO groups can further improve the char layer formation and inhibits the production of VOCs during decomposition, which proves that vapor and condensed phase work together to improve polymer flame retardancy. High temperature char residue of the cured **VSE** and **VDE** at 800 °C achieve 28.0% and 34.5%, respectively. This proves that the introduction of C=N also react with the formation of residue for **VSE**. The introduction of the DOPO has enormous influence on the crosslinked network for **VDE** different from the regular crosslinked network of **VSE**, the changes in free volume and crosslink density endow **VDE** with convenient processability while maintain complete mechanical properties at room temperature. It is believed that these bio-based structural–functional integrated epoxy will be widely used in practical applications in the near future and provide new ideas for the design of modern multifunctional flame-retardant thermosetting.

Conflicts of interest

There are no conflicts to declare.

Acknowledgements

The authors thank the National Natural Science Foundation of China (51703137) and the Fundamental Research Funds for the Central Universities of China (2015SCU11008) for financial support.

Reference

1 Z. Lin, Z. Zeng, X. Gui, Z. Tang, M. Zou and A. Cao, Carbon Nanotube Sponges, Aerogels, and Hierarchical Composites: Synthesis, Properties, and Energy Applications, *Adv. Energy Mater.*, 2016, **6**(17), 1600554.

2 C. Zhang, Y. Chen, H. Li and H. Liu, Facile fabrication of polyurethane/epoxy IPNs filled graphene aerogel with improved damping, thermal and mechanical properties, *RSC Adv.*, 2018, **8**(48), 27390–27399.

3 D. Jiang, V. Murugadoss, Y. Wang, J. Lin, T. Ding, Z. Wang, Q. Shao, C. Wang, H. Liu, N. Lu, R. Wei, A. Subramania and Z. Guo, Electromagnetic Interference Shielding Polymers and Nanocomposites – A Review, *Polym. Rev.*, 2019, **59**(2), 280–337.

4 H. Gu, H. Zhang, J. Lin, Q. Shao, D. P. Young, L. Sun, T. D. Shen and Z. Guo, Large negative giant magnetoresistance at room temperature and electrical transport in cobalt ferrite-polyaniline nanocomposites, *Polymer*, 2018, **143**, 324–330.

5 C. Zhang, J. Y. Huang, S. M. Liu and J. Q. Zhao, The synthesis and properties of a reactive flame-retardant unsaturated polyester resin from a phosphorus-containing diacid, *Polym. Adv. Technol.*, 2011, **22**(12), 1768–1777.

6 S. Wang, S. Q. Ma, C. X. Xu, Y. Liu, J. Y. Dai, Z. B. Wang, X. Q. Liu, J. Chen, X. B. Shen, J. J. Wei and J. Zhu, Vanillin-Derived High-Performance Flame Retardant Epoxy Resins: Facile Synthesis and Properties, *Macromolecules*, 2017, **50**(5), 1892–1901.

7 T. R. Hull, A. Witkowski and L. Hollingbery, Fire retardant action of mineral fillers, *Polym. Degrad. Stab.*, 2011, **96**(8), 1462–1469.

8 A. S. Luyt, S. S. Malik, S. A. Gasmi, A. Porfyris, A. Andronopoulou, D. Korres, S. Vouyiouka, M. Grosshauser, R. Pfaendner, R. Brüll and C. Papaspyrides, Halogen-Free Flame-Retardant Compounds. Thermal Decomposition and Flammability Behavior for Alternative Polyethylene Grades, *Polymers*, 2019, **11**(9), 1479.

9 E. Roze, L. Meijer and A. Bakker, Prenatal Exposure to Organohalogens, Including Brominated Flame Retardants, Influences Motor, Cognitive, and Behavioral Performance at School Age, *Environ. Health Perspect.*, 2009, **117**(12), 1953–1958.

10 K. S. Betts, New Thinking on Flame Retardants, *Environ. Health Perspect.*, 2008, **116**(5), A210–A213.

11 B. A. Babalola and A. A. Adeyi, Levels, dietary intake and risk of polybrominated diphenyl ethers (PBDEs) in foods commonly consumed in Nigeria, *Food Chem.*, 2018, **265**, 78–84.

12 X. Xu, S. Ma, J. Wu, J. Yang, B. Wang, S. Wang, Q. Li, J. Feng, S. You and J. Zhu, High-performance, command-degradable, antibacterial Schiff base epoxy thermosets: synthesis and properties, *J. Mater. Chem. A*, 2019, **7**(25), 15420–15431.

13 S.-Y. Lu and I. Hamerton, Recent developments in the chemistry of halogen-free flame retardant polymers, *Prog. Polym. Sci.*, 2002, **27**(8), 1661–1712.

14 Q. Zhang, S. Yang, J. Wang, J. Cheng, Q. Zhang, G. Ding, Y. Hu and S. Huo, A DOPO based reactive flame retardant constructed by multiple heteroaromatic groups and its application on epoxy resin: curing behavior, thermal degradation and flame retardancy, *Polym. Degrad. Stab.*, 2019, **167**, 10–20.

15 I. van der Veen and J. de Boer, Phosphorus flame retardants: Properties, production, environmental occurrence, toxicity and analysis, *Chemosphere*, 2012, **88**(10), 1119–1153.

16 C. H. Lin, T. Y. Hwang, Y. R. Taso and T. L. Lin, Phosphorus-Containing Epoxy Curing Agents *via* Imine Linkage, *Macromol. Chem. Phys.*, 2007, **208**(24), 2628–2641.

17 B. Schartel, U. Braun, A. I. Balabanovich, J. Artner, M. Ciesielski, M. Döring, R. M. Perez, J. K. W. Sandler and V. Altstädt, Pyrolysis and fire behaviour of epoxy systems containing a novel 9,10-dihydro-9-oxa-10-phosphaphenanthrene-10-oxide-(DOPO)-based diamino hardener, *Eur. Polym. J.*, 2008, **44**(3), 704–715.

18 R. Jian, P. Wang, L. Xia and X. Zheng, Effect of a novel P/N/S-containing reactive flame retardant on curing behavior, thermal and flame-retardant properties of epoxy resin, *J. Anal. Appl. Pyrolysis*, 2017, **127**, 360–368.

19 W. Xu, A. Wirasaputra, S. Liu, Y. Yuan and J. Zhao, Highly effective flame retarded epoxy resin cured by DOPO-based co-curing agent, *Polym. Degrad. Stab.*, 2015, **122**, 44–51.

20 X. Wang, Y. Hu, L. Song, W. Xing, H. Lu, P. Lv and G. Jie, Flame retardancy and thermal degradation mechanism of epoxy resin composites based on a DOPO substituted organophosphorus oligomer, *Polymer*, 2010, **51**(11), 2435–2445.

21 H. Qiao, Y. Liang, G. Xu, Y. Zhang, Y. Wang and J. Hu, Preparation of a Novel Phosphorus-Nitrogen Containing Novolac Curing Agent for Epoxy Resin and flame-retardancy of its cured epoxy resin, *Des. Monomers Polym.*, 2019, **22**(1), 171–179.

22 A. Mpoukouvalas, W. Li, R. Graf, K. Koynov and K. Matyjaszewski, Soft elastomers *via* introduction of poly(butyl acrylate)"diluent" to poly(hydroxyethyl acrylate)-based gel networks, *ACS Macro Lett.*, 2012, **2**(1), 23–26.

23 W. Zhang, X. Li and R. Yang, Blowing-out effect in epoxy composites flame retarded by DOPO-POSS and its correlation with amide curing agents, *Polym. Degrad. Stab.*, 2012, **97**(8), 1314–1324.

24 H. Liu, Z.-e. Fu, K. Xu, H.-l. Cai, X. Liu and M.-C. Chen, Preparation and characterization of high performance Schiff-base liquid crystal diepoxide polymer, *Mater. Chem. Phys.*, 2012, **132**(2), 950–956.

25 T. Ahamad and N. Nishat, New antimicrobial epoxy-resin-bearing Schiff-base metal complexes, *J. Appl. Polym. Sci.*, 2008, **107**(4), 2280–2288.

26 P. Xie, H. Li, B. He, F. Dang, J. Lin, R. Fan, C. Hou, H. Liu, J. Zhang, Y. Ma and Z. Guo, Bio-gel derived nickel/carbon nanocomposites with enhanced microwave absorption, *J. Mater. Chem. C*, 2018, **6**(32), 8812–8822.

27 Y. Kong, Y. Li, G. Hu, J. Lin, D. Pan, D. Dong, E. Wujick, Q. Shao, M. Wu, J. Zhao and Z. Guo, Preparation of polystyrene-b-poly(ethylene/propylene)-b-polystyrene grafted glycidyl methacrylate and its compatibility with recycled polypropylene/recycled high impact polystyrene blends, *Polymer*, 2018, **145**, 232–241.

28 J. Lin, X. Chen, C. Chen, J. Hu, C. Zhou, X. Cai, W. Wang, C. Zheng, P. Zhang, J. Cheng, Z. Guo and H. Liu, Durably Antibacterial and Bacterially Antiadhesive Cotton Fabrics Coated by Cationic Fluorinated Polymers, *ACS Appl. Mater. Interfaces*, 2018, **10**(7), 6124–6136.

29 C. Lin, Y. Taso, C. Hsieh, H. Lee, F. Su, A. Tu, K. Hwang, K. Rin, Y. R. Taso, C. W. Hsieh, H. H. Lee, F. H. Su, A. To, K. Ko, A. B. Duh and K. Y. Hwang, New phosphorus-based oxazine compounds, prepared by mixing 2-hydroxy benzaldehyde compound, phenylamine compound and oxa-phospha-phenanthrene-oxide and adding formaldehyde/trioxymethylene, US2009171120-A1, JP2009161504-A, US7566780-B2, TW200927753-A, JP4961361-B2 and TW380991-B1, 2009.

30 M. Ciesielski, A. Schäfer and M. Döring, Novel efficient DOPO-based flame-retardants for PWB relevant epoxy resins with high glass transition temperatures, *Polym. Adv. Technol.*, 2008, **19**(6), 507–515.

31 S. Waśkiewicz, K. Zenkner, E. Langer, M. Lenartowicz and I. Gajlewicz, Organic coatings based on new Schiff base epoxy resins, *Prog. Org. Coat.*, 2013, **76**(7), 1040–1045.

32 K. S. Chen and R. Z. Yeh, Pyrolysis kinetics of epoxy resin in a nitrogen atmosphere, *J. Hazard. Mater.*, 1996, **49**(2), 105–113.

33 S. V. Levchik and E. D. Weil, Thermal decomposition, combustion and flame-retardancy of epoxy resins—a review of the recent literature, *Polym. Int.*, 2004, **53**(12), 1901–1929.

34 M. P. Luda, A. I. Balabanovich, M. Zanetti and D. Guaratto, Thermal decomposition of fire retardant brominated epoxy resins cured with different nitrogen containing hardeners, *Polym. Degrad. Stab.*, 2007, **92**(6), 1088–1100.

35 X. Qian, L. Song, Y. Hu, R. K. K. Yuen, L. Chen, Y. Guo, N. Hong and S. Jiang, Combustion and Thermal Degradation Mechanism of a Novel Intumescent Flame Retardant for Epoxy Acrylate Containing Phosphorus and Nitrogen, *Ind. Eng. Chem. Res.*, 2011, **50**(4), 1881–1892.

36 M. Giamberini, E. Amendola and C. Carfagna, Curing of a rigid rod epoxy resin with an aliphatic diacid: an example of a lightly crosslinked liquid crystalline thermoset, *Macromol. Rapid Commun.*, 1995, **16**(2), 97–105.

37 S. Y. Chan, L. Si, K. I. Lee, P. F. Ng, L. Chen, B. Yu, Y. Hu, R. K. K. Yuen, J. H. Xin and B. Fei, A novel boron–nitrogen intumescent flame retardant coating on cotton with improved washing durability, *Cellulose*, 2018, **25**(1), 843–857.